J Mater Sci (2008) 43:75–82
DOI 10.1007/s10853-007-2091-y

Structural studies of a new electroceramic composite: $Pb(Fe_{0.5}Nb_{0.5})O_3$ (PFN)-$Cr_{0.75}Fe_{1.25}O_3$(CRFO)

F. N. A. Freire · H. H. B. Rocha · M. R. P. Santos · P. B. A. Fechine · F. M. M. Pereira · R. S. T. M. Sohn · I. F. Vasconcelos · A. S. B. Sombra

Received: 11 April 2007 / Accepted: 9 August 2007 / Published online: 26 September 2007
© Springer Science+Business Media, LLC 2007

Abstract A study of the structural characteristics of the composites $[Pb(Fe_{0.5}Nb_{0.5})O_3(PFN)]_x$-$[Cr_{0.75}Fe_{1.25}O_3(CRFO)]_{100-x}$ (x = 0 (CRFO100), 10, 50, 90, 100) was performed in this work. The compounds PFN100 and CRFO100 were prepared by conventional solid-state method and investigated by X-Ray Diffraction (XRD), Scanning Electron Microscopy (SEM), and ^{57}Fe Mössbauer Spectroscopy techniques. The X-ray analysis shows that PFN100 is tetragonal and the CRFO100 phase has a trigonal symmetry. The refinement of all the composites was also performed and discussed in this paper. The Mössbauer spectrum for the composite samples shows a paramagnetic doublet and a sextet probably assigned to a magnetic phase associated to Fe^{+3}. For the sample PFN100, only a magnetic field of 49.5 T (isomer shift (δ) = 0.21 mm/s) was detected. For the composite sample, the δ and Δ are typical of Fe ions at sites of octahedral coordination.

F. N. A. Freire · P. B. A. Fechine · F. M. M. Pereira
Departamento de Química Orgânica e Inorgânica, Universidade Federal do Ceará, Fortaleza, Ceara CEP 60455-760, Brazil

H. H. B. Rocha
Departamento de Engenharia de Teleinformática, Universidade Federal do Ceará, Fortaleza, Ceara CEP 60455-970, Brazil

F. N. A. Freire · H. H. B. Rocha · M. R. P. Santos · P. B. A. Fechine · F. M. M. Pereira · R. S. T. M. Sohn · A. S. B. Sombra (✉)
Laboratório de Telecomunicações e Ciência e Engenharia dos Materiais (LOCEM), Departamento de Física, Universidade Federal do Ceará, Caixa Postal 6030, Fortaleza, Ceara CEP 60455-760, Brazil
e-mail: sombra@fisica.ufc.br
URL: www.locem.ufc.br

I. F. Vasconcelos
Departamento de Engenharia Metalúrgica e de Materiais, Universidade Federal do Ceará, Fortaleza, Ceara CEP 60455-760, Brazil

F. N. A. Freire
Faculdade de Educação, Ciências e Letras do Sertão Central–Curso de Química, Universidade Estadual do Ceará, Quixadá, Ceara CEP 63900-000, Brazil

Introduction

The demands for miniaturization in the microwave communication technologies require continuing discovery and development of new materials [1]. Fabrication of microwave ceramics with high relative dielectric permittivity (or dielectric constant) (ε_r) and good thermostability together with small dielectrics losses in wide temperature and frequency ranges is an actual problem since the application of such materials in the microwave technology ensures reduction of mass and overall dimensions of microwave [2].

A combined study of both the crystal structure and the electro-physical properties of new compounds and solid solutions is necessary for the development of new ceramic material [2]. Physical properties of a material depend upon the microstructures and therefore by controlling the microstructure, materials can be designed (or optimal selected instead, in agreement with [3], according to desirable properties [4]. Effective synthesis techniques providing reproducibility in commercial production of high electro-physical parameters of ceramic materials and of microwave elements based on them have to be developed.

$Pb(Fe_{1/2}Nb_{1/2})O_3$ (PFN), a lead-based complex perovskite, is regarded as a good candidate as a multilayer ceramic capacitor owing to its high dielectric constant and low sintering temperature [5].

Multilayer ceramic capacitors, because of their large capacitance, highly compact design, and reliability, have

become promising candidates for electronic devices. Alkaline earth titanate barium titanate for example $BaTiO_3$ and its solid solutions have been traditionally used for this application for almost five decades [6].

The polycrystalline ceramic $Cr_{0.75}Fe_{1.25}O_3$ (CRFO) [7] is a member of hematite (α-Fe_2O_3) and eskolaite (Cr_2O_3) system ($Cr_YFe_{2-Y}O_3$, $Y = 0.75$). Hematite and eskolaite were classified as anti-ferromagnetic insulators [8] and as high resistivity similar to that of Cu_2O [9]. They present a continuous solid solution in the entire concentration range [10, 11], that is characteristic of corundum oxides [8]. Both the end members of the series are anti-ferromagnetically ordered at room temperature (α-Fe_2O_3 below Néel temperature $T_N = 682°C$, Cr_2O_3 $T_N = 27°C$), however the spin ordering in these oxides has different symmetry and is markedly weaker in Cr_2O_3 [8]. Results on the Mössbauer spectra was measured in the range of $Y = 0$ to $Y = 2$ [8].

The single-phase ceramic of PFN [$Pb(Fe_{0.5}Nb_{0.5})O_3$] has been reported difficult to produce because of the appearance of stable pyrochlore phases (i.e., $Pb_3Nb_4O_{13}$ and $Pb_2Nb_2O_7$ after calcinations). To avoid the formation of pyrochlore in PMN, Swartz and Shrout [12, 13] proposed a two-stage calcinations route. It consists of two calcinations steps; coulumbite precursor is formed first followed by formation of perovskite. The amount of pyrochlore phase is greatly reduced. In the work of Lejeune and Boilot [14], pure PFN powder is obtained after the mixture of 4PbO, Fe_2O_3, and Nb_2O_5 is processed at 850 °C for 16 h. Shrout et al. [13] prepared PFN powders by first mixing and reacting Fe_2O_3 and Nb_2O_5 at 1,000 °C for 4 h to form $FeNbO_4$. Then, $FeNbO_4$ reacts with PbO at temperature ranging from 750 °C to 800 °C for 4 h.

Perovskite lead-based solid solutions were reported to be sintered at temperature range of 850–1100 °C [14, 15]. Stoichiometric $Pb(Fe_{0.5}Nb_{0.5})O_3$ (PFN) perovskite ceramics produced by reaction-sintering process were investigated [16]. Lead iron niobate is one of the family of lead-based complex perovskites, which is of interest as a component in commercial electronic ceramic materials because of its high relative permittivity and low sintering temperature [17]. Many investigations have been carried out on the microwave dielectric properties of modified lead iron niobates perovskites by A-site or B-site substitution [18, 19]. $CaTiO_3$ modified $Pb(Fe_{0.5}Nb_{0.5})O_3$ dielectrics were prepared by solid-state process and the structure analysis was performed together with the dielectric characterization [20].

In this work is reported the preparation of the PFN100 and CRFO100 ceramics through the solid state route and uses these materials to prepare the composite samples. The samples were studied through X-ray diffraction, Scanning Electron Microscopy (SEM), and Mössbauer Spectroscopy techniques. The production and study of the properties of the composite PFN-CRFO is important in view of possible applications in microwave and RF devices based in high dielectric constant materials.

Experimental methods

In the CRFO phase, detailed in [7], study we choose to follow the ytrium iron garnet stoichiometry ($Y_3Fe_5O_{12}$) and for phase PFN, we choose to follow perovskite stoichiometry $PbTiO_3$.

$$\begin{aligned} Y_3Fe_5O_{12} &\equiv Cr_3Fe_5O_{12} \\ &= Cr_{0.75}Fe_{1.25}O_3 \rightarrow Cr_YFe_{2-Y}O_3 \\ &\quad (\mathrm{CRFO}, Y = 0.75) \end{aligned} \tag{1}$$

$$\begin{aligned} PbTiO_3 &= Pb(Fe_{0.5}Nb_{0.5})O_3 \rightarrow Pb(Fe_xNb_x)O_3 \\ &\quad (\mathrm{PFN},\ X = 0.5) \end{aligned} \tag{2}$$

Polycrystalline samples of PFN and CRFO, whose chemical composition is given by the formulae $Cr_{0.75}Fe_{1.25}O_3$ and $Pb(Fe_{0.5}Nb_{0.5})O_3$, respectively, were synthesized by conventional solid-state reaction methods. Reagents oxides were accurately weighed in stoichiometric amounts of Fe_2O_3 (Aldrich, 99+%) and Cr_2O_3 (Reagen, 99.8%) for CRFO, and Fe_2O_3 (Aldrich, 99+%), Nb_2O_5 (Aldrich 99+%) and PbO (Aldrich, 99.9+%) for PFN. The starting materials were hand-ground in an agate mortar. Prior to the first heat treatment, high-energy ball milling of the homogeneous powder mixture hand-grounded was conducted in a planetary ball mill (Fritsch Pulverisette 6). The rotation speed of the disks carrying the sealed vials was 400 rpm. Milling of powder samples was done at room temperature in stainless steel vial (volume $\sim$ 110 mL) using 20 stainless steel balls (4 g and 10 mm diameter). The time of the mechanical milling operation was 60 min. This operation was merely used to give an improved homogeneity to the powder. Subsequently, the mixtures of oxide were calcined in conventional controlled furnaces (Rapid Temp Furnace/Eurotherm 2404 and EDG 1800/EDGCON3P) at 1,570 K for 5 h to synthesize CRFO100 in atmospheric air. A solid-state reaction process with the columbite precursor method [14], where the raw powder had high purity (more than 99%), was used to synthesize PFN. The $FeNbO_4$ phase was first synthesized at 1,370 K for 3 h in atmospheric air, then the $Pb(Fe_{0.5}Nb_{0.5})O_3$ powder was synthesized by a mixture of $FeNbO_4$ and PbO, where the calcination was done in the same conventional controlled furnaces 1,320 K for 3 h. After calcination, we added about 5 wt% of an organic binder (glycerine). For the PFN100 phase, only glycerine was added in the oxide mixture (2 wt%). The PFN and CRFO was used to prepare the composites PFN(X): PFN100 (X = 100 (100%PFN + 0%CRFO), PFN90 (X = 90(90%PFN + 10%

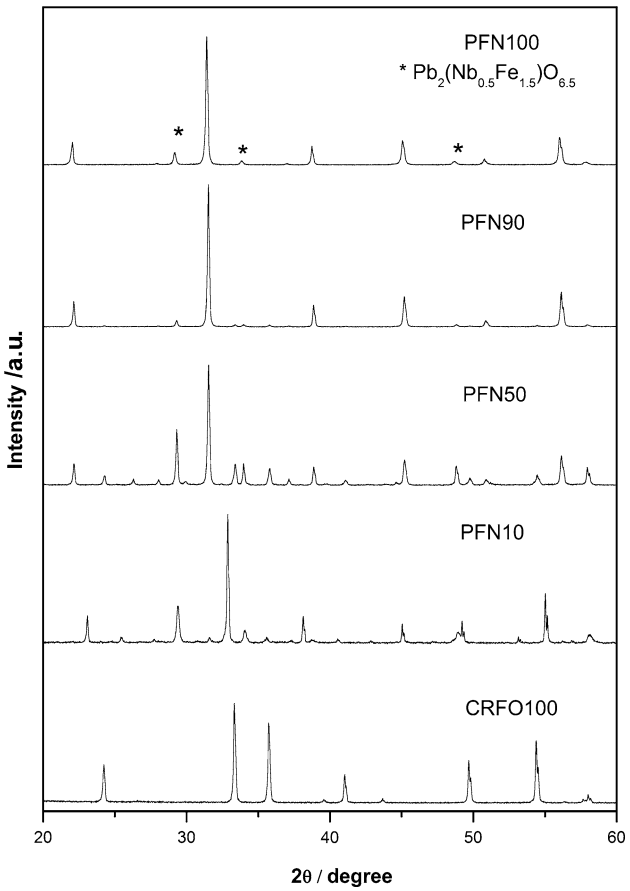

Fig. 1 XRD patterns of composite samples PFN100, PFN90, PFN50, PFN10, CRFO100. [*($Pb_2(Nb_{0.5}Fe_{1.5})O_{6.5}$)]

Table 1 CRFO100: atomic positions (X, Y, Z), refined isotropic thermal parameters (B) and site occupancies (S_0)

Átom	Wyckoff position	X	Y	Z	B	S_0
Fe1	12c	0.000000	0.000000	0.353012	3.3467	0.625
Cr1	12c	0.000000	0.000000	0.353012	0.0000	0.375
O1	18e	0.695898	0.000000	0.250000	1.9626	1.000

Table 2 PFN100: atomic positions (X, Y, Z), refined isotropic thermal parameters (B) and site occupancies (S_0)

Átom	Wyckoff Position	X	Y	Z	B	S_0
Pb	1a	0.000000	0.000000	0.004000	0.0000	1.000
Nb	1b	0.500000	0.500000	0.500000	0.0000	0.500
Fe1	1b	0.500000	0.500000	0.500000	0.0000	0.500
O1	1b	0.500000	0.500000	0.030000	0.0000	1.000
O2	1c	0.500000	0.000000	0.492000	0.5000	1.000

CRFO)) PFN50 (X = 50(50%PFN + 50%CRFO)), PFN10 (X = 10 (10%PFN + 90%CRFO)), and CRFO100(X = 0 (0%PFN + 100%CRFO)). They were uniaxially pressed (270 MPa) into pellets in a steel die. The pellets, whose typical dimensions were 4.4 mm in diameter and 2 mm in thickness, were sintered at 1,120 K for 3 h in atmospheric air.

Table 3 Numerical criteria of fit and density

Sample	R_P (%)	R_{WP} (%)	R_B (%)	S_{Gof}	d_{DW}	Density (g/cm^3)
PFN100	10.89	14.32	6.04	1.25	0.75	8.417
PFN90	11.60	16.02	5.68	1.23	0.55	7.038
PFN50	11.47	16.27	5.91	1.16	1.31	6.897
PFN10	13.29	17.31	7.29	1.23	0.96	5.561
CRFO100	7.77	10.57	3.62	1.37	0.71	5.255

X-ray diffraction

The X-ray powder diffraction profiles of the prepared samples were recorded using a powder X-ray diffractometer system Rigaku D/max-B, composed of X-ray generator, X-ray optics and goniometer, X-ray detector and counting system, and recorder for data recording or storing [20]. Powder samples were fixed on a silicon plate with silicon paste. Patterns were collected at laboratory temperature (about 294 K) using Cu Kα radiation at 40 kV and 25 mA in the geometry of Bragg-Brentano, in steps of 0.02° 2θ at 2 s/ step, ranging from 20° to 60° (2θ).

In the present study, the Rietveld's powder structure refinement analysis [21–23] of X-ray powder diffraction data is adopted to obtain the refined structural parameters, such as atomic coordinates, lattice parameters, thermal parameters, etc. The Rietveld's software DBWS-9807a [24] is specially designed to refine the structural parameters through a least-squares method. The peak shape was assumed to be pseudo-Voigt (pV) function with asymmetry. The background of each pattern was fitted by a polynomial function of degree 5. Refinements were conducted without refining the anisotropic atomic thermal parameters or occupancies.

The least-square procedures were adopted for minimization of the difference between the observed and simulated powder diffraction pattern. The minimization was carried out by using the reliability index parameters R_{WP} (weighted residual error) and Durbin-Watson d-statistic d_{DW}. The refinement continues till convergence is reached with the value of the quality factor Goodness of fit (S_{GoF}) very close to 1 (varies between 1.23 and 1.37), which confirms the goodness of refinement.

Scanning Electron Microscopy

The scanning electron microscopy combined with energy dispersive analysis used in the study of ceramics is

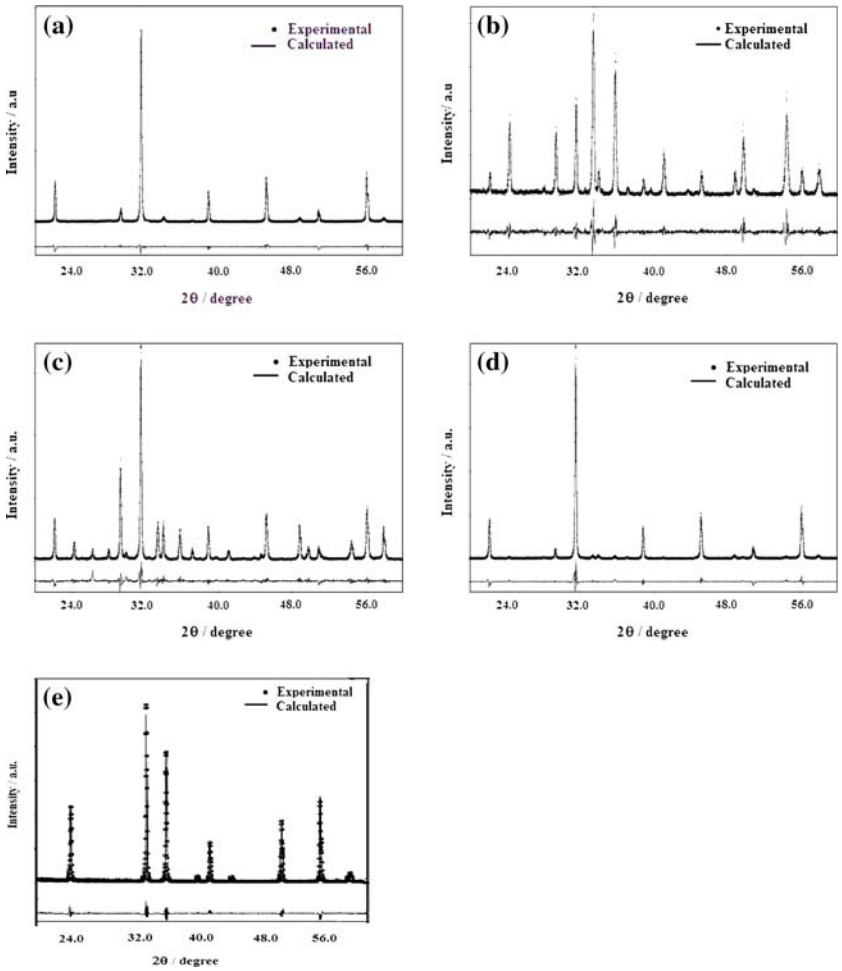

Fig. 2 The diffraction pattern of sample (**a**) PFN100 (**b**) PFN10 (**c**) PFN50 (**d**) PFN90 (**e**) CRFO100 The dotted line is the experimental pattern and the straight line is the calculated pattern. The differences are shown below them

Table 4 Comparison between the nominal percentage used in the sample preparation and the data obtained from the Quantitative Phase Analysis (QPA), without internal standard

Sample	PFN100		CRFO100	
	Nominal %	AQF	Nominal %	AQF
PFN90	90	92.70	10	7.30
PFN50	50	55.02	50	44.98
PFN10	10	11.53	90	88.47

generally of morphological interest. By scanning an electron probe across a specimen, high-resolution images of the specimen with very high magnifications was obtained. Compositional analysis of a material also was obtained by monitoring secondary X-rays produced by electron-specimen interaction. The microstructure observation and compositional analysis of the sintered surface of the cylindrical specimens, covered with a thin layer of carbon, was performed by scanning electron microscopy, on a scanning electron microscope, Phillips XL-30, equipped with an EDS detector EDAX-CDU Leap Detector.

^{57}Fe Mössbauer Spectroscopy

The Mössbauer spectra were obtained in standard transmission geometry, using a constant acceleration spectrometer with a radioactive source of ^{37}Co in Rh matrix. Measurements were carried out at room temperature on powder samples. The spectra were evaluated using the Normos fitting routine which makes use of a set of Lorentzian, and computes the contribution of each curve to the total absorption spectrum, by least square procedure. All the isomer shifts (δ) quoted are relative to metallic iron (α-Fe).

Results and discussion

Rietveld analysis

The XRD patterns of PFN100, PFN90, PFN50, PFN10, CRFO100 composite samples are shown in Fig. 1. In the Rietveld procedure, a model based on iron oxide [25] and chromium oxide [26] was used for CRFO100, is

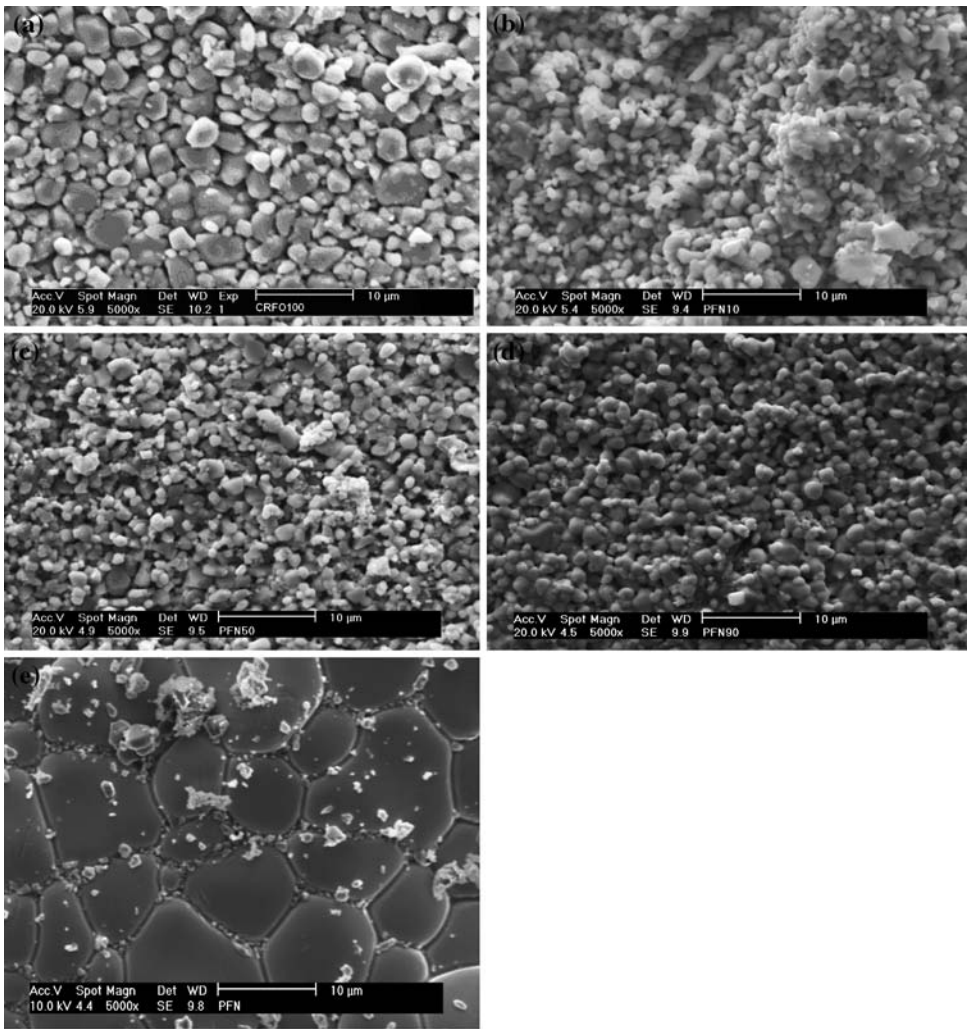

Fig. 3 SEM micrographs of the samples: (**a**) CRFO100; (**b**) PFN10; (**c**) PFN50; (**d**) PFN90; and (**e**) PFN100

summarized in Table 1. The structural and thermal parameters for the PFN100 are summarized in Table 2. In Table 3 the data obtained from the Rietveld procedure associated to PFN and CRFO compounds are collected.

The CRFO presents at room temperature, a trigonal structure belonging to group $R\bar{3}c$ (#167), with six molecules in the unity cell ($Z = 6$). In the structure, the iron and chromium are localized in the Wyckoff Positions 12c, where the oxygen ion occupies the site 18e (Table 1). The refinement is illustrated in Fig. 2e.

In Fig. 2a, we have the refinement of PFN100. To a first approximation, this major phase has a tetragonal perovskite type structure, space group P4mm (JCPDS file #88-356) with cell parameter $a = b = 4.0116$ Å, $c = 4.007$ Å. The additional reflection (marked by *) is correlated with a pyrochlore phase of lead niobium oxide, $Pb_2(Nb_{0.5}Fe_{1.5})O_{6.5}$ (JCPDS file # 39-888). This phase has a cubic structure with cell parameter $a = 10.5486$ Å.

In Fig. 2b–d we have the numerical and experimental diffraction of the samples PFN10, PFN50, and PFN90, respectively. The major numerical criteria of fit for this analyze were R_{wp}, R_B, S_{Gof}, and d_{DW} (see Table 3).

In Table 4, we have the Quantitative Phase Analysis (QPA) without internal standard, of the samples obtained from the refinement procedure. One can observe that the QPA is in good agreement for the composites phase in the sample of PFN10, PFN50, and PFN90. The Rietveld's method was useful for determination of quantitative phase abundances of the composite materials. In this procedure, only the phases PFN100 and CRFO100 were considered. The existence of pyrochlore phase [$Pb_2(Nb_{0.5}Fe_{1.5})O_{6.5}$] is probably the responsible for observed variance of the results.

Scanning electron microscopy

The grain morphology of the samples was investigated by Scanning Electron Microscopy (SEM). In Fig. 3, we present micrography of samples (a) CRFO100, (b) PFN10,

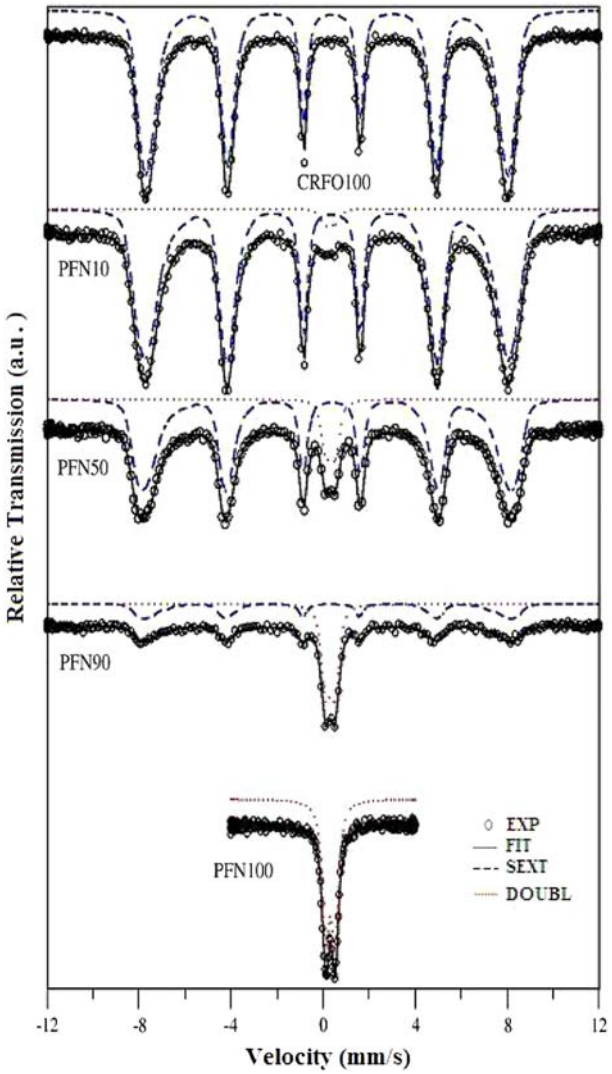

Fig. 4 Mössbauer spectra of the composite samples CRFO100; PFN10; PFN50, PFN90, and PFN100 at room temperature

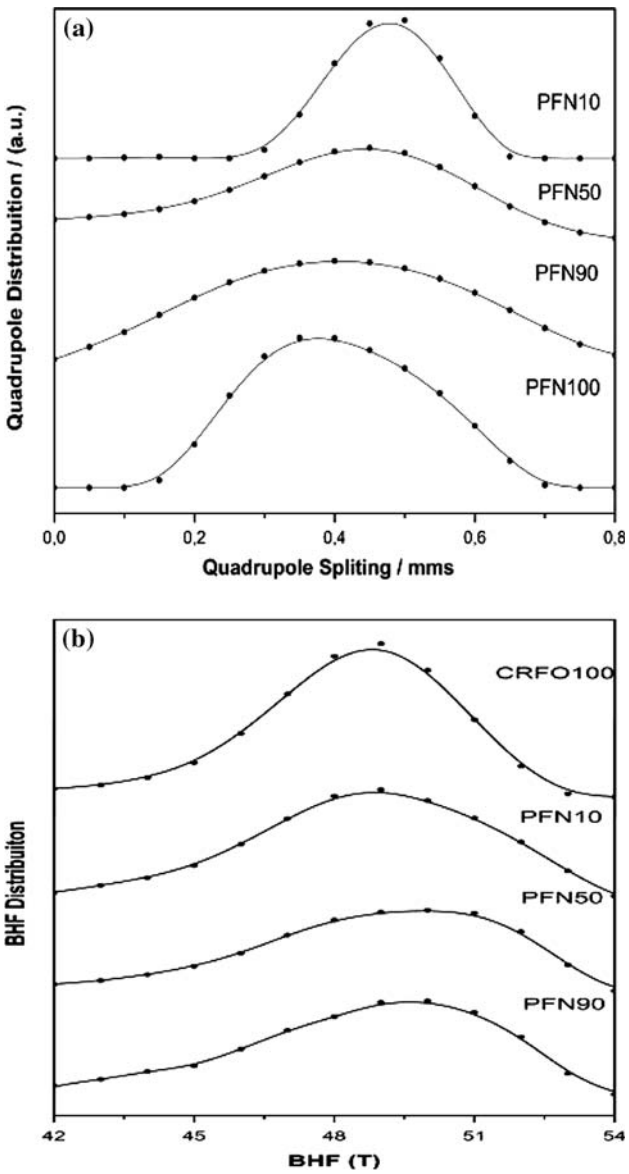

Fig. 5 (**a**) Quadrupole splitting and (**b**) hiperfine magnetic field distributions for samples associated to Table 5 and Fig. 5

(c) PFN50, (d) PFN90, and (e) PFN100. For CRFO100 sample, one can notice a large variety of morphologies like aggregates and polygonal shapes. For the PFN50 sample, polygonal shapes for the grains are observed. We observe diversity in the grain size distribution, with long cylindrical grains, for example. In the case of the PFN100, microscopy showed larger grain sizes with polygonal shapes.

^{57}Fe Mössbauer spectroscopy

Room temperature Mössbauer spectra for the CRFO100 sample show one well resolved sextet from the iron atoms in the octahedral coordination (Fig. 4), and one well resolved doublet from iron in tetragonal coordination for PFN100 sample. The prepared composites contain both contributions: one sextet and one doublet. It shows that the distribution of particles size is not uniform. Besides, the relative spectral areas of these sextets and doublets were found to be satisfactorily fitted, being proportional to the amounts of the Fe ion-probe in these compounds. This could support the hypothesis that a meaningful solid state reaction could not have occurred between CRFO100 and PFN100 phases, during the synthesis treatment.

The quadrupolar distribution curves showed in Fig. 5a, indicates that the Fe ion-probe in the paramagnetic phase is in the Fe^{3+} oxidation state and octahedral configuration, over the entire final mixture for all samples. This suggests that the composites preserve the electrical and magnetic properties of both components. The average value of the

Table 5 Mössbauer parameters

Specimen	Average of QUA over the distribution		Average of BHF over the distribution	
	Δ mm/s	δ mm/s	BHF T	δ mm/s
PFN 100	0.40	0.31(±0.01)	–	–
PFN 90	0.40	0.30(±0.01)	49.5	0.15(±0.04)
PFN 50	0.45	0.31(±0.01)	49.5	0.21(±0.02)
PFN 10	0.47	0.26(±0.02)	49.0	0.22(±0.01)
CRFO 100	–	–	48.5	0.22(±0.01)

Table 6 Areas of the fitted curves relative to magnetic phases

Sample	Nominal		Experimental (Mössbauer) %	
	Magnetic phase (CRFO100)	Paramagnetic phase (PFN100)	Magnetic phase (CRFO100)	Paramagnetic phase (PFN100)
PFN90	92.5%	7.5%	92.4%	7.7%
PFN50	83.2%	16.8%	83.5%	16.5%
PFN10	71.8%	28.2%	73.5%	26.5%

quadrupole distribution presents for PFN100 every broad, with a peak value around $\Delta = 0.40$ mm/s (see Table 5). The study of isomer shift (δ) gives information on valence state and chemical bonding of the sample. The isomer shift value is $\delta = 0.31$ mm/s which is characteristic of an octahedral coordination (see Table 5 and Fig. 5a). For the Fe^{3+} state, the δ is typically in the range 0.20–0.32 mm/s [27].

The hyperfine field (BHF) for the CRFO100 sample (Fig. 5b) indicates the most probable value BHF = 48,5 T, and a symmetrical and regular distribution over the 45–53 T interval. For the others samples (in Fig. 5b) we observe the same shape, with the most probable value BHF = 49.5 T, over the ±4 T interval. This suggests that the magnetic order is similar for these samples, and that the phases have preserved their magnetic properties, after the synthesis treatment described previously. We have attributed the 49–48 T decreasing in the most probable value, to a larger distance between the magnetic domains for the mixture.

The areas of the fitted curves relative to magnetic phases (see Table 6) are showing that the experimental and nominal values are very close.

Conclusions

In this article we did a study of the structural characteristics of the composites $[Pb(Fe_{0.5}Nb_{0.5})O_{3z}(PFN)]_z$-$[Cr_{0.75}Fe_{1.25}O_3(CRFO)]_{100-x}$. The compounds were prepared by the conventional solid-state method and they were studied using X-Ray Diffraction (XRD), Scanning Electron Microscopy (SEM), and ^{57}Fe Mössbauer Spectroscopy.

The PFN phase is a Tetragonal perovskite in the spatial group P4mm (JCPDS file #88-356), but we observed the formation of a pyrochlore phase (lead niobium oxide, $Pb_2(Nb_{0.5}Fe_{1.5})O_{6.5}$). The CRFO phase belongs to a trigonal structure in the space group $R\bar{3}c$ (#167).

The refinement analysis of all the composites $Z = 10$, 50, and 90 were performed and discussed. The Quantitative Phase Analysis (QPA) of the samples, obtained from the refinement procedure, was obtained and we can observe a good agreement for the composition of each composite phase. The existence of pyrochlore phase ($Pb_2(Nb_{0.5}Fe_{1.5})O_{6.5}$) is probably responsible for observed variance of the results.

The SEM analysis shows that for the CRFO100 sample a large variety of morphologies like aggregates and polygonal shape is observed. For the PFN50 sample, polygonal shapes for the grains are observed. We also observe that the grain size distribution is broader with long cylindrical grains. In the case of the PFN100, microscopy showed larger grain sizes with polygonal shapes.

The Mössbauer spectra show the superposition of a wide sextet and a doublet for the composite samples. For the CRFO100, the experimental spectrum has a magnetic sextet and for PFN100 a doublet. The Mössbauer spectra for the individual spectra is proportional to the amounts of the Fe ion-probe in these compounds.

Acknowledgements This work was partly sponsored by CAPES, FUNCAP and CNPq (Brazilian agencies) and the US Air Force Office of Scientific Research (AFOSR) (FA9550-06-1-0543).

References

1. Su WF, Lin SC (2003) J Eur ceram Soc 23:2593
2. Nenasheva EA, Kartenko NF (2001) J Eur ceram Soc 21:2697
3. Jansen M, Schön JC (2004) Nat Mater 3:838
4. Bid S, Pradhan SK (2004) Mater Chem Phys 84:291
5. Anata S, Thomas NW (1999) J Eur Ceram Soc 19:1873
6. Herbert JM (1995) Ceramic Dieletric and Capacitors, Eletrocomponent Science Monographs, vol 6. Gordon and Breach, NY
7. Rocha HHB, Freire FNA, Silva RR, Gouveia DX, de Paiva JAC, Sasaki JM, Santos MRP, Góes JC, Sombra ASB, Structural Studies of the magneto-dieletric composite: $Cr_{0.75}Fe_{1.25}O_3$ (CRFO)-$Fe_{0.5}Cu_{0.75}Ti_{0.75}O_3$ (FCTO) submitted
8. Grygar T, Bezdic P, Dedecek JD, Pretovský E, Schneeweiss O (2003) Ceramic-Silikáty 47(1):32
9. Onari S, Arai T, Kudo K (1977) Physic Rev B 16(4):1717
10. Grygar T, Bezdicka P, Gaspary EG (1999) J Eletrochem Soc 146:3234
11. Steinwehr HHV (1967) Kristalogr 125:377
12. Swartz SL, Shrout TR (1982) Mater Res Bull 17:1245
13. Shrout TR, Swartz SL, Haum MJ (1984) Am Ceram Soc Bull 63(6):808

14. Lejeune M, Boilot JP (1982) Ceram Int 8(3):99
15. Mohan D, Prasad R, Bannerjee S (1996) J Mater Sci Lett 15:2149
16. Kagata H, Kato J, Nishimoto K, Inoue T (1993) Jpn J Appl Phys 32:4332
17. Kucheiko S, Choi J-W, Kim H-J, Yoon S-J, Jung H-J (1997) J Am Ceram Soc 80(11):2937
18. Zhao H, Zhou J, Bai Y, Gui Z, Li L (2004) J Magn Magn Mater 208:280
19. Pardavi-Horvarth M (2000) J Magn Magn Mater 215–216:174
20. The New Standard of X-ray Diffractometer. MultiFlex (2000) The Rigaku J 17(2):10
21. Rietveld HM (1967) Acta crystallogr 2:65
22. Rietveld HM (1969) J Appl Crystallogr 2:65
23. Young RA (1996) The Rietveld Method. Oxford University Press/IUCr, Oxford, pp 1–38
24. Young RA, Sakthivel A, Moss TS, Paiva-Santos CO (1995) J Appl Cryst 28:366
25. Hill RJ, Flack HD (1987) J Appl Crystallogr 20:356
26. Hu X, Chen XM, Wu SY (2003) J Eur ceram Soc 23:1919
27. Dyar MD (1985) Am Mineral 70:304